Point-gap bound states in non-Hermitian systems

Zixi Fang [1,2] Chen Fang,[1,3,4,*] and Kai Zhang [1,5,†]

[1]*Beijing National Laboratory for Condensed Matter Physics, and Institute of Physics,*
Chinese Academy of Sciences, Beijing 100190, China
[2]*School of Physical Sciences, University of Chinese Academy of Sciences, Beijing 100049, China*
[3]*Songshan Lake Materials Laboratory, Dongguan, Guangdong 523808, China*
[4]*Kavli Institute for Theoretical Sciences, Chinese Academy of Sciences, Beijing 100190, China*
[5]*Department of Physics, University of Michigan Ann Arbor, Ann Arbor, Michigan 48109, USA*

In this paper, we systematically investigate impurity-induced bound states in one-dimensional non-Hermitian systems. By establishing the relationship between bound-state energy and the requisite impurity potential, we conveniently construct an impurity potential diagram corresponding to point gaps. This diagram indicates both the minimal impurity potential required to generate bound states within each point gap and the distribution of bound states across these point gaps for a given impurity potential. From this, we reveal that a finite impurity potential is required to generate bound states in the absence of Bloch saddle points; otherwise, even a negligible impurity potential can yield bound states. Additionally, we show that bound states in point gaps with nonzero spectral winding numbers are sensitive to boundary conditions and abruptly shift to the edges upon opening the boundaries, signifying the bulk-boundary correspondence in point-gap topology.

I. INTRODUCTION

When a system interacts with external environments, such as optical systems with balanced gain and loss [1–6] or quasiparticle excitations with a finite lifetime [7–9], its nonunitary time evolution or broadened spectral function necessitates an effective non-Hermitian Hamiltonian description [10–15]. Recently, many intriguing phenomena emerged in non-Hermitian band systems, with a major focus on the non-Hermitian skin effect (NHSE) [16–40]. This effect is characterized by the condensation of the majority of system eigenstates on its boundary when open boundary conditions (OBCs) are imposed. These localized eigenstates can be quantitatively described using the generalized Brillouin zone (GBZ) that is made of complex momenta [18,21,25,27].

Impurities are common in realistic materials and significantly responsible for their transport properties [41]. For instance, doping impurities in semiconductors enhance conductivity [42], and magnetic impurities in metals lead to the Kondo effect [43]. This importance motivates the investigation of impurity states in non-Hermitian systems [44–50]. It was known that NHSE manifests as a boundary phenomenon in non-Hermitian systems, and impurities with codimension-1 can be treated as a soft boundary [38,51]. Given this connection, it is natural to ask whether NHSE influences the formation of impurity bound states. Moreover, impurities serving as soft boundaries can be applied to investigate the bulk-boundary correspondence [52–58].

In non-Hermitian band systems, the complex eigenvalues enrich the types of energy gaps [14,15]. It allows us to assign a spectral winding number to each point gap when the periodic boundary condition (PBC) is applied. Previous studies revealed that NHSE has a point-gap topological origin [25,26], i.e., the collapse of a point gap with a nonzero spectral winding number leads to the emergence of NHSE under OBCs. Therefore, an additional question arises whether bound states in point gaps can reflect the bulk-boundary correspondence regarding point-gap topology in non-Hermitian systems.

In this paper, we present a general theory of impurity-bound states in one-dimensional (1D) non-Hermitian lattice systems, utilizing the Green's function method to establish the exact relationship between the strength of the impurity potential and the corresponding bound-state energy. We reveal that in the absence of Bloch saddle points [59], a finite threshold for the impurity potential is required to generate bound states; otherwise, even an infinitesimal impurity potential can result in bound states, highlighting the crucial role of Bloch saddle points in determining the minimum impurity potential necessary for the appearance of bound states. Here, the Bloch saddle points are defined as the momenta k_s at which $\partial_k \mathcal{H}(k_s) = 0$. Moreover, the envelope of the bound state exhibits asymmetric localization away from the impurity site when NHSE is present, as illustrated in Fig. 1(d). Additionally, we show that a single impurity can confine multiple bound states, among which those residing in the point gaps with nonzero spectral winding number are sensitive to boundary conditions and are pushed to the edges when OBCs are applied, indicating the presence of NHSE.

———————
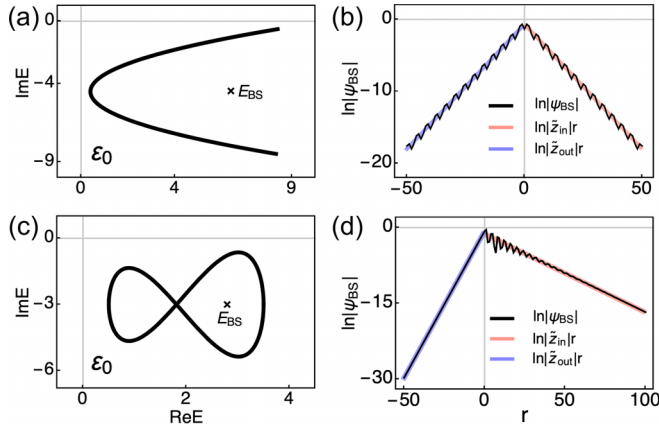*cfang@iphy.ac.cn
†phykai@umich.edu

FIG. 1. (a) and (c) represent the PBC spectra (the black curves) as well as the bound-state energy E_{BS} located in the point gaps (the black asterisk). (b) and (d) show the logarithm of the amplitude of two bound states (the black lines), that is, $\ln|\tilde{z}_{in}|r$ (the red line) on the right side ($r + 1 > 0$) and $\ln|\tilde{z}_{out}|r$ (the blue line) on the left side ($r + 1 < 0$). The Hamiltonian parameters $\{t_{-2}, t_{-1}, t_0, t_1, t_2\}$ in Eq. (6) are set to be $\{-2, -2, 4.4 - 4.5i, 2, -2\}$ for (a) and (b) and $\{-1, 1/2, 2 - 3i, 1, 1\}$ for (c) and (d).

II. FORMATION OF BOUND STATES IN NON-HERMITIAN SYSTEMS

We start with a general single-band tight-binding model under PBCs, of which the Hamiltonian can be expressed as

$$H_0 = \sum_r \sum_{l=-m}^{n} t_l |r\rangle\langle r+l| = \sum_{k \in BZ} \mathcal{H}_0(z \equiv e^{ik})|k\rangle\langle k|, \quad (1)$$

with $\mathcal{H}_0(z) = \sum_{l=-m}^{n} t_l z^l$ a Laurent polynomial of z, r representing the lattice site, and t_l indicates the hopping parameter that only depends on the (finite) hopping range l due to the translation symmetry. As momentum k transverses the entire BZ, the corresponding PBC spectrum forms arcs or loops, denoted as σ_{PBC}, which divides the complex energy plane into several disconnected regions called point gaps [13,15] and labeled as $\mathcal{E}_0, \mathcal{E}_1, \ldots$. We always specify $\mathcal{E}_0$ as the point gap connected to infinity, as illustrated in Figs. 1(a) and 1(c).

Consider a single impurity at the center of the 1D periodic chain,

$$V = \lambda \sum_r \delta(r)|r\rangle\langle r|, \quad (2)$$

where λ represents the strength of the impurity potential and assumes a complex value [4]. The single-impurity potential can produce bound states that are localized around the impurity site and have energies within point gaps, as shown in Figs. 1(a) and 1(c). The eigen wave function $\psi_E(r)$ with energy E in the full Hamiltonian $H = H_0 + V$ can be determined using Green's function [60], that is,

$$\psi_E(r) = \lambda \psi_E(0) G_0(E; r), \quad (3)$$

where $G_0(E; r) = \langle r|1/(E - H_0)|0\rangle$ with H_0 under PBC. Here, $\psi_E(0)$ is known by the normalization condition of $\psi_E(r)$. Based on the Hamiltonian in Eq. (1), the Green's

function can be further expressed in an integral form,

$$G_0(E; r) = \oint_C \frac{dz}{2\pi i} \frac{z^{r+m-1}}{P_E(z)}, \quad (4)$$

where m indicates the multiplicity of the pole in $\mathcal{H}_0(z)$ and $P_E(z) = z^m(E - \mathcal{H}_0(z))$ represents an non-negative-order polynomial with respect to z for a given energy E. Under PBC, the integral contour C, namely BZ, is the unit circle $|z| = 1$ in the complex z plane. Therefore, for a given point-gap energy E_{BS} produced by the impurity potential of strength λ, the corresponding bound state can be calculated as

$$\psi_{BS}(r) = \lambda \, \psi_{BS}(0) \begin{cases} \sum_{|z|<1} R(E_{BS}, z)z^r, & r+m-1>0, \\ \sum_{|z|>1} -R(E_{BS}, z)z^r, & r+m-1<0, \end{cases}$$
$$(5)$$

where m represents the multiplicity of the pole in the Hamiltonian $\mathcal{H}_0(z)$ and is therefore a finite number; $R(E_{BS}, z_i) = -z_i^{m-1}/t_n \prod_{j(\neq i)=1}^{m+n} 1/(z_i - z_j)$ is the residue of the function $[z(E_{BS} - \mathcal{H}_0(z))]^{-1}$ at its pole z_i. Note that these poles correspond to zeros of $P_{E_{BS}}(z)$ in Eq. (4). Here, the bound states refer to the right wave functions of the total Hamiltonian, the spatial localization of which essentially arises from the spatial correlation described in Eq. (4). Hence, the biorthogonal basis is necessary when extended to more complicated multiband cases (see more details in the Supplemental Material [60]). It can be derived from Eq. (5) that bound states exhibit exponential localization; when away from the impurity site, the localization behavior on the right (left) side of the impurity is dominated by the largest (smallest) poles inside (outside) $|z| = 1$.

Here, we consider two examples, one without NHSE [Figs. 1(a) and 1(b)] and another with NHSE [Figs. 1(c) and 1(d)], to show that the presence of NHSE results in asymmetric decay behaviors for the bound states. The model Hamiltonian is composed of the free part

$$\mathcal{H}_0(z) = t_{-2}z^{-2} + t_{-1}z^{-1} + t_0 + t_1 z + t_2 z^2 \quad (6)$$

and the impurity potential in Eq. (2) with strength λ. The bound states are created with an impurity potential $\lambda = 15$ in Fig. 1(a) and $\lambda = 5.5$ in Fig. 1(c). To better characterize the localization behavior, we plot $\ln|\psi_{BS}(r)|$ for the bound state in each case, marked by the black lines in Figs. 1(b) and 1(d), which matches well with the straight lines of slopes $\ln|\tilde{z}_{in}|$ (the red line) on the right side of the impurity site and $\ln|\tilde{z}_{out}|$ (the blue line) on the left side. Here, $|\tilde{z}_{in}|$ ($|\tilde{z}_{out}|$) represents the largest (smallest) magnitude of the poles within (out) $|z| = 1$. The slope of the bound state, $\partial_r \ln|\psi_{BS}(r)|$, is merely the inverse of decay length and dominated by these two dominant poles. As a result, the comparison between Figs. 1(b) and 1(d) demonstrates that in the case of NHSE, the bound state exhibits an asymmetric decay behavior away from the impurity.

III. NONZERO THRESHOLD OF IMPURITY POTENTIAL FOR BOUND STATES

To further investigate the bound states in different point gaps, we establish the exact relationship between single-impurity potential λ and its bound-state energy E_{BS}.

Remarkably, we reveals that the absence of the Bloch saddle point necessitates a finite threshold of impurity potential for the formation of bound states; otherwise, an infinitesimal impurity potential can excite bound states.

Combining Eqs. (3) and (4), one can obtain the relation between the impurity potential λ and the corresponding bound-state energy E_{BS}, that is,

$$\lambda^{-1}(E_{\mathrm{BS}}) = \sum_{|z_i|<1} \mathrm{R}(E_{\mathrm{BS}}, z_i), \tag{7}$$

which gives the strength of the impurity potential λ required for producing the bound state with energy E_{BS}. Since the bound-state energy E_{BS} is not included in the σ_{PBC}, there are no poles touching $|z| = 1$, ensuring the above relation is always well defined. For each point gap $\mathcal{E}_i$, we can assign a spectral winding number [25] for $\mathcal{H}_0(z)$ regarding the bound-state energy,

$$\forall E_{\mathrm{BS}} \in \mathcal{E}_i, \quad w_{\mathrm{BZ},\mathcal{E}_i} = n_z - n_p, \tag{8}$$

where $n_p = m$ is the multiplicity of the pole in $\mathcal{H}_0(z)$, and n_z is the number of zeros of $E_{\mathrm{BS}} - \mathcal{H}_0(z)$ inside the BZ, depending on the choice of bound-state energy E_{BS}. Note that the zeros exactly correspond to the counted poles in Eq. (7). Therefore, when E_{BS} lies in the point gaps $\mathcal{E}_i$ with $w_{\mathrm{BZ},\mathcal{E}_i} = n$ or $-m$, all poles are included either inside or outside the trajectory $|z| = 1$, which causes the right-hand side of Eq. (7) to vanish and requires an infinite impurity potential to create bound states. Here, n and m represent the longest hopping range to the left and right in the Hamiltonian $\mathcal{H}_0(z)$, respectively. Therefore, we reach the first conclusion: The bound states cannot be created within point gaps that possess spectral winding of n and $-m$. Two examples are presented in Figs. 2(a) and 2(c) and Figs. 2(b) and 2(d), respectively. The point gaps where bound states cannot appear are labeled as $\mathcal{E}_4$ ($w_{\mathrm{BZ},\mathcal{E}_4} = -m = -2$) in Fig. 2(a) and $\mathcal{E}_1$ ($w_{\mathrm{BZ},\mathcal{E}_1} = n = 1$) in Fig. 2(b).

We now examine the minimum impurity potentials that can yield bound states within different point gaps. The minimum bound-state energy shall be in the point gaps and close to the PBC spectrum σ_{PBC}. We begin with $E_{\mathrm{BS}} \in \mathcal{E}_i$ and let it approach $E \in \sigma_{\mathrm{PBC}}$, as illustrated in Figs. 2(a) and 2(b), the corresponding impurity potential $\lambda(E_{\mathrm{BS}})$ in Eq. (7) reaches a limit value, as shown in Figs. 2(c) and 2(d). Likewise, for each point gap $\mathcal{E}_i$, we can define the set of minimum impurity potentials required to create bound states in this point gap,

$$\Lambda_{\mathcal{E}_i} := \{ \lim_{E_{\mathrm{BS}} \to E} \lambda(E_{\mathrm{BS}}) | E_{\mathrm{BS}} \in \mathcal{E}_i, E \in \sigma_{\mathrm{PBC}} \}. \tag{9}$$

As illustrated in Fig. 2(a), there are four disjoint point gaps $\mathcal{E}_{i=0,1,2,3}$ that allow for bound states. Relating to these point gaps, we identify four sets of minimum impurity potentials derived from Eq. (9), $\Lambda_{\mathcal{E}_{i=0,1,2,3}}$, i.e., four different colored boundary curves in Fig. 2(c). When the impurity potential λ is inside the gray region surrounded by $\Lambda_{\mathcal{E}_0}$ in Fig. 2(c), it is insufficiently strong to give rise to bound states. As λ surpasses the boundary $\Lambda_{\mathcal{E}_0}$, bound states first appear in the point gap $\mathcal{E}_0$. As shown in Fig. 2(c), generating bound states in other point gaps necessitates even larger impurity potentials. If λ goes into the colored region, e.g., the red region encircled by $\Lambda_{\mathcal{E}_1}$, multiple bound states are produced, one in the point gap $\mathcal{E}_1$ and another [not shown in Fig. 2(a)] in the
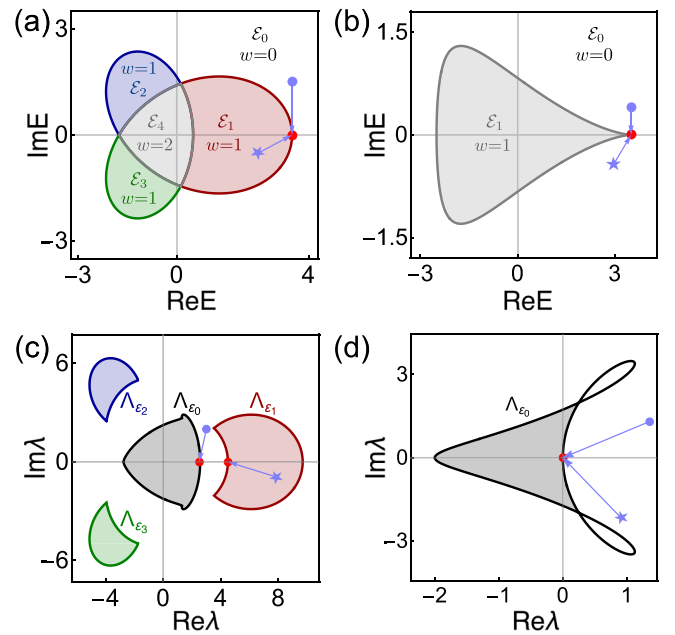

FIG. 2. Comparison between two examples: (a), (c) without and (b), (d) with a Bloch saddle point. (a) and (b) show the disjoint point gaps $\mathcal{E}_i$ separated by the PBC spectra. Each point gap is labeled by the assigned spectral winding number. (c) and (d) illustrate the diagram of impurity potential λ, which includes several regions bounded by $\Lambda_{\mathcal{E}_i}$ corresponding to point gap $\mathcal{E}_i$. For instance, when bound-state energies in point gap $\mathcal{E}_i$, as indicated by blue dots or stars in (a) and (b), approach the PBC spectra (the red dots), the requisite impurity potentials λ, denoted by blue dots or stars in (c) and (d), correspondingly reach the boundaries $\Lambda_{\mathcal{E}_i}$ (the red dots). The Hamiltonian parameters in Eq. (5) are $\{t_{-2}, t_{-1}, t_1\} = \{2, 1/2, 1\}$ for (a) and (c) and $\{1/2, 1, 2\}$ for (b) and (d).

$\mathcal{E}_0$. More details about the λ diagram are presented in the Supplemental Material [60]. Therefore, the finite gray area covering the origin $\lambda = 0$ in Fig. 2(c) indicates a finite threshold of impurity potentials required to generate point-gap bound states.

While Hamiltonian $H_0(z)$ exhibits a Bloch saddle point, an infinitesimal impurity potential can excite bound states. We define the Bloch saddle point as the saddle point with a unit modulus that satisfies $\partial_z \mathcal{H}_0(z)|_{z=z_s} = 0$ and $|z_s| = 1$ simultaneously. The energy at the Bloch saddle point is denoted as $E_s = \mathcal{H}_0(z_s)$. One example with a Bloch saddle point is shown in Figs. 2(b) and 2(d). When E_{BS} approaches $E_s \in \sigma_{\mathrm{PBC}}$, as illustrated in Fig. 2(b), there are at least two poles in Eq. (7), denoted as z_{s1} inside $|z| = 1$ and z_{s2} outside $|z| = 1$, that are closest to each other with the distance $\delta z_s = |z_{s1} - z_{s2}|$ and coincide exactly at the Bloch saddle point ($\delta z_s = 0$) [60]. Consequently, the inverse of the impurity potential $\lambda^{-1}(E_{\mathrm{BS}})$ in Eq. (7) is dominated by the residue $\mathrm{R}(E_{\mathrm{BS}}, z_{s1}) \propto 1/\delta z_s$. Based on Eq. (9), the minimum impurity potential is attained at a Bloch saddle point energy, $\Lambda_{\mathcal{E}_0}(E_s) = \lim_{E_{\mathrm{BS}} \to E_s} \lambda(E_{\mathrm{BS}}) \approx \delta z_s \to 0$, which means that an infinitesimal impurity potential λ can excite the bound states with energies near E_s. The set of minimum impurity potentials $\Lambda_{\mathcal{E}_0}$ for the point gap $\mathcal{E}_0$ is shown in Fig. 2(d), which is composed of three segments connected by two self-intersections. Thus,

zero threshold of the impurity potential means the curve $\Lambda_{\mathcal{E}_0}$ crosses $\lambda = 0$, as shown in Fig. 2(d). More details for this example are presented in the Supplemental Material [60]. Comparing with the case in Figs. 1(a) and 1(c), we conclude the following: When the Hamiltonian lacks a Bloch saddle point, a finite impurity potential is needed to excite the bound states; otherwise, an infinitesimal impurity potential can produce bound states with energies near the Bloch saddle-point energy.

IV. SENSITIVITY OF POINT-GAP BOUND STATES TO BOUNDARY CONDITIONS

It has been known that the point gaps, characterized by nonzero spectral winding in Eq. (8), will collapse when OBCs are imposed. What happens to the bound states in these point gaps when the boundary condition changes from PBC to OBC? Here, we demonstrate that these point-gap bound states exhibit a sensitivity to boundary conditions and are driven towards the boundaries following the collapse of the point gap at that bound-state energy.

The transition between boundary conditions can be parametrized by the boundary link strength s under the Hamiltonian $H_0^s = H_0 - s H_B$, where H_0 indicates the PBC Hamiltonian and H_B represents the boundary hopping terms. As the parameter s goes from 0 to 1, the Hamiltonian H_0^s is modulated from PBC to OBC; correspondingly, the integral contour C in Eq. (4) undergoes a continuous deformation from BZ into GBZ with the intermediary trajectory denoted as C_s [60]. In this process, the trajectory C_s sweeps through the blue shaded region shown in Fig. 3(b), that is, the difference between the interiors of BZ and GBZ. We label the intermediary spectrum as $\sigma_s := \{\mathcal{H}_0(z) | z \in C_s, 0 < s < 1\}$ and the OBC spectrum as σ_{OBC}. After introducing the impurity potential V defined in Eq. (2), the total Hamiltonian becomes $H^s = H_0^s + V$, and impurity states can appear. Here, we define the inverse of decay length of the impurity state with energy E on the right side of the impurity site as

$$\kappa_+ := \partial_r \ln |\psi_E(r)|, \quad r + 1 > 0. \tag{10}$$

Under the boundary condition with a boundary link s, it can be derived from Eq. (5) that the localization behavior of the impurity state with energy E is dominated by the largest poles included by C_s instead of $|z| = 1$. Meanwhile, the relation between the bound-state energy and requisite impurity potential can be obtained from Eq. (7), where the residue is summed over the poles within the interior of trajectory C_s rather than BZ.

An illustrative example is shown in Fig. 3, and the Hamiltonian under PBC ($s = 0$) is the same as that in Fig. 2(a). We start from two bound states within different point gaps. One bound state with energy marked as E_1 (the red cross) in Fig. 3(a) resides in the point gap $\mathcal{E}_1$. Two poles of $(E_1 - \mathcal{H}_0(z))^{-1}$ within GBZ are labeled as $z_{1,2}$ [the red dots in Fig. 3(b)]. The spectral winding number $w_{\mathrm{BZ}, \mathcal{E}_1} = -1$ in Eq. (8) means that only one pole z_2 is located in the intermediary region between BZ and GBZ. As the boundary conditions change from PBC to OBC, C_s deviates from BZ, traverses the pole z_2 within the shaded region ($s = s_c$) shown in Fig. 3(b),
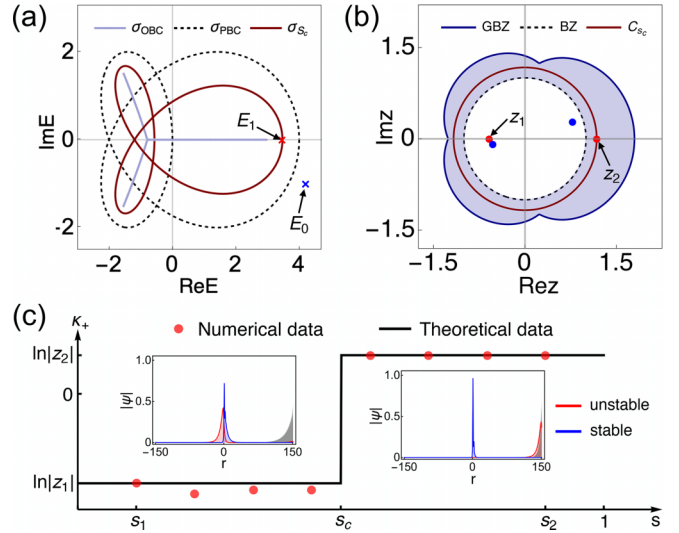

FIG. 3. (a) The spectra under different boundary conditions and the two bound-state energies E_0 and E_1, marked by the blue and red crosses. (b) BZ, GBZ, and critical trajectory C_{s_c} that crosses the pole z_2. The red and blue dots denote the poles related to E_1 and E_0, respectively. (c) The inverse of decay length κ_+ for $\psi_{E_1}(r)$ experiences one jump at $s = s_c$. Two insets show the spatial profiles of impurity states with the boundary link $s_1 = 1 - 10^{-9}$ and $s_2 = 1 - 10^{-30}$, respectively. For comparison, the bulk states shown by the gray profiles are localized on the edge once $s \neq 0$. The system parameters in $\mathcal{H}_0(z)$ are the same as Fig. 2(a).

and eventually enters GBZ. Before and after the transition ($s = s_c$), the dominant pole enclosed by C_s will be changed. As a result, κ_+ for the bound state with energy E_1 experiences a jump, as shown in Fig. 3(c). Correspondingly, the bound state $\psi_{\mathrm{BS}}(r)$ transitions into an edge mode with a diverging amplitude ($\kappa_+ > 0$) under a large-size limit, as illustrated by the red profile in the insets of Fig. 3(c). It exhibits that the bound state in the point gap with nonzero spectral winding is unstable and sensitive to the boundary conditions. In contrast, the bound state with energy E_0, labeled by the blue cross in Fig. 3(a), stays in the point gap $\mathcal{E}_0$. Due to the zero spectral winding number of $\mathcal{E}_0$, the trajectory C_s does not across any (blue) poles for $0 \leqslant s \leqslant 1$, as shown in Fig. 3(b). Therefore, this point-gap bound state is stable during the change in boundary conditions, indicated by the blue profile in the insets of Fig. 3(c).

In general cases, we start from a bound state $\psi_{\mathrm{BS}}(r)$ with the energy E_{BS} inside the point gap $\mathcal{E}_i$ under PBC ($s = 0$), and examine its localization behavior as the boundary conditions vary from PBC to OBC. Suppose that the point gap has a spectral winding $w_{\mathrm{BZ}, \mathcal{E}_i} = q$, as defined in Eq. (8), the BZ contains $n_p + q$ poles in Eq. (7), while GBZ always encloses n_p poles [25]. There are q poles distributed in the intermediary region between BZ and GBZ. As the boundary condition varies from PBC ($s = 0$) to OBC ($s = 1$), the spectrum σ_s traverses the energy E_{BS} q times before finally collapsing into the OBC spectrum σ_{OBC}. Accordingly, the trajectory C_s sweeps q poles as it deforms from BZ into GBZ, resulting in the inverse of decay length κ_+ experiencing q abrupt changes. One example with $q = 2$ is shown in the Supplemental Material [60]. The

number of jumps in κ_+ exactly corresponds to the spectral winding number $w_{\mathrm{BZ},\varepsilon_i} = q$ of the point gap, indicating the bulk-edge correspondence regarding the point-gap topology.

V. CONCLUSIONS

In summary, we investigate the interplay between point gaps and bound states induced by a single impurity within 1D non-Hermitian lattice systems. We establish the exact relationship between the bound-state energy and required impurity potential and reveal the critical role of the Bloch saddle point on the minimum threshold of impurity potentials. Specifically, in the absence of a Bloch saddle point, a finite impurity potential is required for the generation of bound states; otherwise, an infinitesimal potential is sufficient to create bound states with energies close to that of the Bloch saddle point. Meanwhile, we show that the presence of NHSE causes the asymmetric localization length of bound states. We demonstrate that the bound states within the point gaps characterized by nonzero spectral winding are unstable and sensitive to boundary conditions. The sensitivity of point-gap bound states indicates the bulk-edge correspondence of the point-gap topology specific to non-Hermitian systems.

[1] A. Regensburger, C. Bersch, M.-A. Miri, G. Onishchukov, D. N. Christodoulides, and U. Peschel, Nature (London) **488**, 167 (2012).

[2] T. Gao, E. Estrecho, K. Y. Bliokh, T. C. H. Liew, M. D. Fraser, S. Brodbeck, M. Kamp, C. Schneider, S. Höfling, Y. Yamamoto, F. Nori, Y. S. Kivshar, A. G. Truscott, R. G. Dall, and E. A. Ostrovskaya, Nature (London) **526**, 554 (2015).

[3] L. Feng, R. El-Ganainy, and L. Ge, Nat. Photon. **11**, 752 (2017).

[4] R. El-Ganainy, K. G. Makris, M. Khajavikhan, Z. H. Musslimani, S. Rotter, and D. N. Christodoulides, Nat. Phys. **14**, 11 (2018).

[5] M.-A. Miri and A. Alù, Science **363**, eaar7709 (2019).

[6] Ş. K. Özdemir, S. Rotter, F. Nori, and L. Yang, Nat. Mater. **18**, 783 (2019).

[7] V. Kozii and L. Fu, arXiv:1708.05841.

[8] H. Shen and L. Fu, Phys. Rev. Lett. **121**, 026403 (2018).

[9] Y. Nagai, Y. Qi, H. Isobe, V. Kozii, and L. Fu, Phys. Rev. Lett. **125**, 227204 (2020).

[10] V. M. Martinez Alvarez, J. E. Barrios Vargas, M. Berdakin, and L. E. F. Foa Torres, Eur. Phys. J.: Spec. Top. **227**, 1295 (2018).

[11] E. J. Bergholtz, J. C. Budich, and F. K. Kunst, Rev. Mod. Phys. **93**, 015005 (2021).

[12] Y. Ashida, Z. Gong, and M. Ueda, Adv. Phys. **69**, 249 (2020).

[13] K. Ding, C. Fang, and G. Ma, Nat. Rev. Phys. **4**, 745 (2022).

[14] Z. Gong, Y. Ashida, K. Kawabata, K. Takasan, S. Higashikawa, and M. Ueda, Phys. Rev. X **8**, 031079 (2018).

[15] K. Kawabata, K. Shiozaki, M. Ueda, and M. Sato, Phys. Rev. X **9**, 041015 (2019).

[16] T. E. Lee, Phys. Rev. Lett. **116**, 133903 (2016).

[17] V. M. Martinez Alvarez, J. E. Barrios Vargas, and L. E. F. Foa Torres, Phys. Rev. B **97**, 121401(R) (2018).

[18] S. Yao and Z. Wang, Phys. Rev. Lett. **121**, 086803 (2018).

[19] F. K. Kunst, E. Edvardsson, J. C. Budich, and E. J. Bergholtz, Phys. Rev. Lett. **121**, 026808 (2018).

[20] S. Yao, F. Song, and Z. Wang, Phys. Rev. Lett. **121**, 136802 (2018).

[21] K. Yokomizo and S. Murakami, Phys. Rev. Lett. **123**, 066404 (2019).

[22] C. H. Lee and R. Thomale, Phys. Rev. B **99**, 201103(R) (2019).

[23] C. H. Lee, L. Li, and J. Gong, Phys. Rev. Lett. **123**, 016805 (2019).

[24] S. Longhi, Phys. Rev. Res. **1**, 023013 (2019).

[25] K. Zhang, Z. Yang, and C. Fang, Phys. Rev. Lett. **125**, 126402 (2020).

[26] N. Okuma, K. Kawabata, K. Shiozaki, and M. Sato, Phys. Rev. Lett. **124**, 086801 (2020).

[27] Z. Yang, K. Zhang, C. Fang, and J. Hu, Phys. Rev. Lett. **125**, 226402 (2020).

[28] Y. Yi and Z. Yang, Phys. Rev. Lett. **125**, 186802 (2020).

[29] L. Xiao, T. Deng, K. Wang, G. Zhu, Z. Wang, W. Yi, and P. Xue, Nat. Phys. **16**, 761 (2020).

[30] A. Ghatak, M. Brandenbourger, J. van Wezel, and C. Coulais, Proc. Natl. Acad. Sci. USA **117**, 29561 (2020).

[31] T. Helbig, T. Hofmann, S. Imhof, M. Abdelghany, T. Kiessling, L. W. Molenkamp, C. H. Lee, A. Szameit, M. Greiter, and R. Thomale, Nat. Phys. **16**, 747 (2020).

[32] L. Li, C. H. Lee, S. Mu, and J. Gong, Nat. Commun. **11**, 5491 (2020).

[33] K. Kawabata, N. Okuma, and M. Sato, Phys. Rev. B **101**, 195147 (2020).

[34] C. C. Wanjura, M. Brunelli, and A. Nunnenkamp, Nat. Commun. **11**, 3149 (2020).

[35] W.-T. Xue, M.-R. Li, Y.-M. Hu, F. Song, and Z. Wang, Phys. Rev. B **103**, L241408 (2021).

[36] L. Li, S. Mu, C. H. Lee, and J. Gong, Nat. Commun. **12**, 5294 (2021).

[37] K. Zhang, Z. Yang, and C. Fang, Nat. Commun. **13**, 2496 (2022).

[38] K. Zhang, C. Fang, and Z. Yang, Phys. Rev. Lett. **131**, 036402 (2023).

[39] S. Longhi, Phys. Rev. Lett. **128**, 157601 (2022).

[40] Y.-M. Hu, H.-Y. Wang, Z. Wang, and F. Song, arXiv:2210.13491.

[41] N. M. R. Peres, Rev. Mod. Phys. **82**, 2673 (2010).

[42] S. T. Pantelides, Rev. Mod. Phys. **50**, 797 (1978).

[43] J. Kondo, Prog. Theor. Phys. **32**, 37 (1964).

[44] N. Hatano and D. R. Nelson, Phys. Rev. Lett. **77**, 570 (1996).

[45] N. Hatano and D. R. Nelson, Phys. Rev. B **56**, 8651 (1997).

[46] L. Li, C. H. Lee, and J. Gong, Commun. Phys. **4**, 42 (2021).

[47] Y. Liu and S. Chen, Phys. Rev. B **102**, 075404 (2020).

[48] Y. Liu, Y. Zeng, L. Li, and S. Chen, Phys. Rev. B **104**, 085401 (2021).

[49] F. Roccati, Phys. Rev. A **104**, 022215 (2021).

[50] Z. Gong, M. Bello, D. Malz, and F. K. Kunst, Phys. Rev. Lett. **129**, 223601 (2022).

[51] C. W. Hsu, B. Zhen, A. D. Stone, J. D. Joannopoulos, and M. Soljačić, Nat. Rev. Mater. **1**, 16048 (2016).

[52] J. C. Y. Teo and C. L. Kane, Phys. Rev. B **82**, 115120 (2010).

[53] C.-K. Chiu, J. C. Y. Teo, A. P. Schnyder, and S. Ryu, Rev. Mod. Phys. **88**, 035005 (2016).

[54] R.-J. Slager, L. Rademaker, J. Zaanen, and L. Balents, Phys. Rev. B **92**, 085126 (2015).

[55] J. D. Sau and E. Demler, Phys. Rev. B **88**, 205402 (2013).

[56] E. J. Meier, F. A. An, and B. Gadway, Nat. Commun. **7**, 13986 (2016).

[57] S.-S. Diop, L. Fritz, M. Vojta, and S. Rachel, Phys. Rev. B **101**, 245132 (2020).

[58] D. S. Borgnia, A. J. Kruchkov, and R.-J. Slager, Phys. Rev. Lett. **124**, 056802 (2020).

[59] N. W. Ashcroft and N. D. Mermin, *Solid State Physics* (Cengage Learning, Boston, 2022).

[60] See Supplemental Material at http://link.aps.org/supplemental/10.1103/PhysRevB.108.165132 for (i) a general theory of bound states in one-dimensional non-Hermitian lattices; (ii) correspondence between bound states and point gaps; (iii) relation between Bloch saddle points and the threshold of the impurity potential; and (iv) sensitivity of bound states to boundary conditions.